This is the preprint version of article http://doi.org/10.1002/pip.3509

Temperature-dependent performance of silicon heterojunction solar cells with transition-metal-oxide-based selective contacts

Anh Huy Tuan Le[1*], Julie Dréon[2], Mathieu Boccard[2], James Bullock[3], Jesús Ibarra Michel[3], Nino Borojevic[1], and Ziv Hameiri[1]

[1]School of Photovoltaic and Renewable Energy Engineering, University of New South Wales, Sydney, NSW 2052, Australia

[2]Photovoltaics and Thin-Film Electronics Laboratory (PV-lab), Institute of Microengineering (IMT), École Polytechnique Fédérale de Lausanne (EPFL), Rue de La Maladière 71b, CH-2002, Neuchâtel, Switzerland

[3]Department of Electrical and Electronic Engineering, University of Melbourne, Victoria 3010, Australia

[*] Corresponding author
Email: leanh619@gmail.com (Anh Huy Tuan Le)

Abstract

The temperature coefficient (TC) is an essential figure of merit to accurately evaluate solar cell performance at various operating temperatures, and hence, enabling the comparison between different cell technologies. Recently, solar cells that use passivating contacts based on transition metal oxide (TMO) layers have attracted much attention due to their excellent performance. Therefore, knowledge of their TCs and insights into their performance at various operating temperatures are of significant interest.

In this study, we investigate the temperature-dependent performance of solar cells with TMO-based passivating contacts at various illumination intensities. We then compare their performance to that of the standard silicon heterojunction (SHJ) solar cells. The efficiency TC (TC_{η}) of solar cells that use passivating contacts based on molybdenum oxide (MoO_x) and titanium oxide (TiO_x) films are found to be almost identical. Both are better than the TC_{η} of the standard SHJ cells and greatly superior to those of cell structures without passivating contacts. The superior TC_{η} of the MoO_x-based cells is mainly due to their favourable TCs of the short-circuit current density (TC_{Jsc}) and fill factor (TC_{FF}), whereas the superiority of TC_{η} of the TiO_x-based cells is solely resulting from the superior TC_{FF}. The favourable TC_{Jsc} of the MoO_x-based cells is explained by an enhanced spectral response at short wavelengths with increasing temperature, due to the improvement of the passivation quality of the MoO_x-based passivating contacts. The beneficial TC_{FF} of both solar cells are partly resulting from the improvement of the contact resistivity of the TMO-based passivating contacts which counterbalances some of the fill factor losses at elevated temperatures. Although an improvement of the passivation quality of the TMO-based passivating contacts is observed at elevated temperature, it does not have a strong impact on the open-circuit voltage TC (TC_{Voc}) of the investigated solar cells. Furthermore, we also found that the studied cells are less sensitive to temperature variation at higher illumination intensities.

Keywords: SHJ, MoO_x, TiO_x, TMO, passivating contacts, temperature coefficient, temperature dependence, silicon solar cells.

1. Introduction

Photovoltaic devices operate under a wide range of temperatures [1]; however, they are often characterized and optimized only at standard testing conditions (STC; at 25 °C with an irradiance of 1000 W/m^2 under the AM1.5G solar spectrum). Since the temperature sensitivity of various cell technologies is different [2], the temperature coefficient (TC) is an essential figure of merit to evaluate the cell performance at different operating temperatures and to allow a more in-depth comparison between various cell technologies [2-4]. The performance of silicon (Si) solar cells is typically reduced with increasing temperature, which is mainly attributed to the reduction of the cell's open-circuit voltage (V_{oc}) [5]. In general, the higher the cell's V_{oc}, the better the open-circuit voltage TC (TC_{Voc}), and hence the efficiency TC (TC_{η}) [5]. To achieve a favourable TC_{η}, cell structures enabling a high V_{oc} are therefore desired [5].

Recent studies have demonstrated the capability of solar cells that integrate passivating contacts to achieve high efficiencies [6-11]. Such contacts are typically composed of two layers: (1) films that provide surface passivation, and (2) films that ensure carrier selectivity, whereas the latter can also contribute to passivation [12-14]. Therefore, passivating contacts enable a significant reduction of the recombination losses at the Si interfaces and an effective collection of only one type of charge carrier [12-14]. Cell structures that integrate these contacts usually exhibit a high V_{oc} [9, 15-18], and hence, they are expected to have a favourable TC_{η}. This was confirmed by our recent study demonstrating that the TC_{η} of solar cells with polysilicon passivating contacts is superior to those of cell structures without passivating contacts [19, 20]. It highlights the advantage of using solar cells that integrate passivating contacts in the field.

Besides polysilicon passivating contacts, passivating contacts based on transition metal oxide (TMO) films have also attracted much attention due to their excellent performance [10, 11]. Depending on the work function, these contacts can be used as hole- or electron-selective collectors [14]. For hole-selective contacts, molybdenum oxide (MoO_x) [11, 21], vanadium oxide (V_2O_x) [22, 23], and tungsten oxide (WO_x) [22, 24] are often used due to their high work functions. Meanwhile, titanium oxide (TiO_x) [10, 25] and tantalum oxide (Ta_2O_x) [26, 27] are integrated into Si solar cells as electron-selective contacts due to their low work function. It is noteworthy that many of the high-efficiency TMO-based solar cells utilize MoO_x and TiO_x films as hole- and electron-selective contacts, respectively [10, 11, 25, 28, 29]. To our knowledge, there is no published report regarding the TC_{η} of these promising solar cells.

In this study, we investigate the temperature-dependent performance of MoO_x- and TiO_x-based solar cells and compare them to that of SHJ cells. We also examine the temperature-dependent behaviour of the surface saturation current density (J_{0s}) and the contact resistivity (ρ_c) of those contacts to gain a deeper understanding regarding their impact on TC_{Voc} and the fill factor TC (TC_{FF}), respectively.

2. Experimental details

2.1. Sample preparation

Textured float zone (FZ) n-type wafers (resistivity: 1.7-2.3 Ω·cm, thickness: 180±10 µm) were used to fabricate solar cells. All the wafers were first Radio Corporation of America (RCA) [30] cleaned and dipped in 1% diluted hydrofluoric (HF) acid. The wafers were then divided into three groups:

1) For the **SHJ cells** (control cells), a stack of 6-nm hydrogenated intrinsic and 6-nm hydrogenated p-doped amorphous Si [a-Si:H(i) and a-Si:H(p), respectively] layers was deposited on the front side using a plasma-enhanced chemical vapor deposition system. A stack of 6-nm a-Si:H(i) and 8-

nm hydrogenated n-doped amorphous Si [a-Si:H(n)] films was formed on the rear side using the same system.

2) For the **MoO_x-based cells**, a 6-nm a-Si:H(i) layer was deposited on the front, followed by a 4-nm thermally evaporated MoO_x film. Their rear structure is identical to that of the SHJ cells.
3) For the **TiO_x-based cells**, the rear side composes a stack of 6-nm a-Si:H(i) film and 1.5-nm TiO_x layer formed by atomic layer deposition while their front structure is identical to that of the SHJ cells.

Additional information regarding the conditions used during the depositions can be found in Ref. [11]. The metallization process of the front contact was similar for the three cell structures. 70-nm indium tin oxide (ITO) film was deposited by a sputtering system through a mask to form active areas of 2 × 2 cm^2. A silver (Ag) grid was then screen-printed on top of the front ITO film, followed by a curing process at 210 °C for the SHJ cells, 130 °C for the MoO_x-base cells, and 160 °C for the TiO_x-based cells for 30 min in air ambient. The rear contacts of the SHJ and MoO_x-based cells were formed by 150-nm sputtered ITO and 100-nm screen-printed Ag layers, whereas that of the TiO_x-based cells composes 1-nm thermally evaporated lithium fluoride (LiF) and 200-nm aluminium (Al) films. Sketches of the investigated devices are shown in Figs. 1(a)-(c).

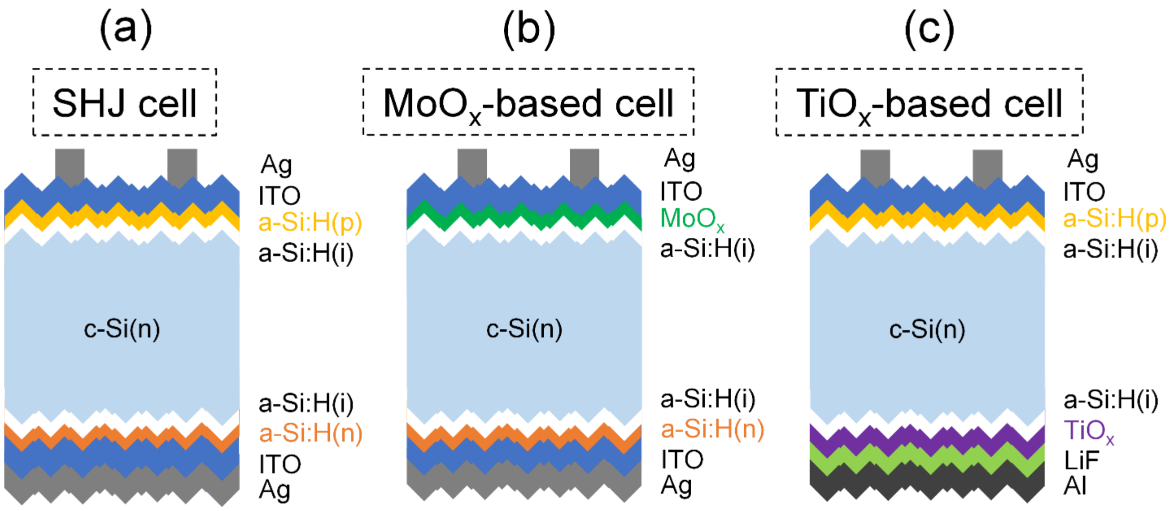

Figure 1: Sketches of (a) standard SHJ, (b) MoO_x-based, and (c) TiO_x-based solar cells used in this study.

To investigate the temperature-dependent behaviour of the MoO_x-and TiO_x-based passivating contacts, symmetrical lifetime structures for effective lifetime (τ_{eff}) measurements and J_{0s} extraction were prepared using n-type FZ textured wafers (1.7-2.3 Ω·cm, 180±10 µm). The lifetime test wafers were passivated with either a-Si:H(i)/MoO_x or a-Si:H(i)/TiO_x stack on both sides.

To extract ρ_c, Cox and Strack [31] test structures were fabricated using both p-type and n-type FZ textured wafers (1.7-2.3 Ω·cm, 180±10 µm). We used p-type wafers for measurements of the MoO_x-based structures to avoid back-to-back diodes. The same layer stacks as for the lifetime test structures were applied to the front side of the Cox and Strack structures, followed by the formation of circular ITO and Ag contacts with different diameters (from 0.02 to 0.8 cm) on top of the MoO_x or TiO_x layer. A full Ag contact was sputtered on the rear side.

The symmetrical lifetime and the Cox and Strack test structures were annealed at 130 °C (for MoO_x-based passivating contacts) and 160 °C (for TiO_x-based passivating contacts) for 30 min in air ambient to mimic the thermal budget of the Ag paste curing process. A similar set (symmetrical lifetime and Cox and Strack test structures) was also prepared for the a-Si:H(i/p)- and a-Si:H(i/n)-based passivating contacts. These test structures were annealed at 210 °C for 30 min in air ambient.

2.2. Characterization

The current-voltage (I-V) parameters of the solar cells are measured from 25 to 70 °C while Suns-V_{oc} measurements are performed by a customized Sinton Suns-V_{oc} system [32] from 80 to 30 °C. The cell's series resistance (R_s) is calculated by comparing the one-sun current density-voltage (J-V) curve to the R_s-free J-V curve obtained from the Suns-V_{oc} measurements [33]. TCs are extracted from the slopes of linear fits of the cell parameters as a function of temperature and are normalized to their values at 25 °C (relative TCs).

The external quantum efficiency (EQE) of the studied solar cells is measured by a solar cell spectral response system (QEX7, PV Measurements Inc.).

Dark I-V measurements are performed on the Cox and Strack structures in the temperature range from 25 to 80 °C to extract ρ_c of the passivating contacts [31]. Note that the rear ohmic contact of these test structures is assumed to have a negligible contribution to the total resistance (R_{tot}). Hence, the obtained ρ_c represents its upper limit.

Sinton lifetime tester (WCT-120TS) is used to measure τ_{eff} as a function of temperature (25 to 80 °C) [34]. J_{0s} is extracted from the τ_{eff} curves using the curve fitting features of Quokka 2 [35] and the approach of Dumbrell *et al.* [36]. The uncertainty in the extracted J_{0s} is calculated from the uncertainty of photoconductance measurements using the approach of McIntosh *et al.* [37]. The models of Schenk [38], Richter *et al.* [39], and Klaassen [40] are used to determine the effective intrinsic carrier concentration ($n_{i,eff}$), the intrinsic lifetime, and the mobility, respectively.

3. Results and discussion

3.1. Temperature-dependent performance of solar cells

The cell parameters of the standard SHJ, MoO_x-, and TiO_x-based solar cells as a function of temperature are presented in Figs. 2(a)-(d). As expected, for all the investigated solar cells, the V_{oc}, fill factor (FF), pseudo fill factor (pFF), and efficiency (η) decrease, whereas the short-circuit current density (J_{sc}) increases at elevated temperatures [5]. The reduction of V_{oc}, FF, and pFF is explained by the increase of $n_{i,eff}$ at elevated temperatures caused by bandgap narrowing [41]. The improvement of J_{sc} can also be explained by the same effect [5].

The V_{oc} of the MoO_x-based cell is comparable to that of the standard SHJ cell at any given temperature. It is expected as both structures integrate a-Si:H(i) layers which are mainly responsible for the surface passivation in these cells [42]. Meanwhile, the lower V_{oc} of the TiO_x-based cell can be explained by the fact that the rear surface passivation was slightly degraded before the TiO_x deposition, since the TiO_x deposition was done in a different facility after a long transportation time of a few weeks.

It is noteworthy that at any given temperature, the J_{sc} of the MoO_x-based cell is higher than that of the standard SHJ cell. This is due to the higher optical bandgap of the MoO_x layer compared to that of a-Si:H(p) film [43-47], resulting in a better spectral response at the short wavelength region (see Fig. 1S). Meanwhile, the J_{sc} of the TiO_x-based cell is lower than that of the standard SHJ cell despite their identical structure at the front side. This can be attributed to the absence of the ITO film at the rear side which can lead to significant parasitic absorption at the metal reflector [48, 49], resulting in a low spectral response at the long wavelength region (see Fig. 1S).

Non-linear behaviour of the temperature-dependent FF in the temperature range from 25 to 40 °C is observed for all the investigated solar cells. The occurrence of this phenomenon has been reported for standard SHJ [2, 50-52] and MoO_x-based passivating contact solar cells [53]; however, it has not been reported for TiO_x-based passivating contact solar cells yet. This trend is often attributed to thermionic barriers at the heterojunctions of these cells [2, 52]. The decrease of *FF* of the MoO_x- and TiO_x-based solar cells in the temperature range from 40 to 70 °C is less pronounced compared to that of the SHJ solar cell. It should be pointed out that for all the cells, the decreasing trend of the *FF* is different from that of the *pFF* as a function of temperature. This difference can be used to assess the contribution of R_s to the temperature-dependent behaviour of *FF*, as will be discussed in Section 3.3.

Compared to the performance of state-of-the-art devices using MoO_x-based passivating contacts at STC, our MoO_x-based cell shows comparable V_{oc} and J_{sc} while its FF is lower by 4.06% [11]. For the TiO_x-based cell, our cell parameters are slightly lower than those of the state-of-the-art devices reported in Ref. [27].

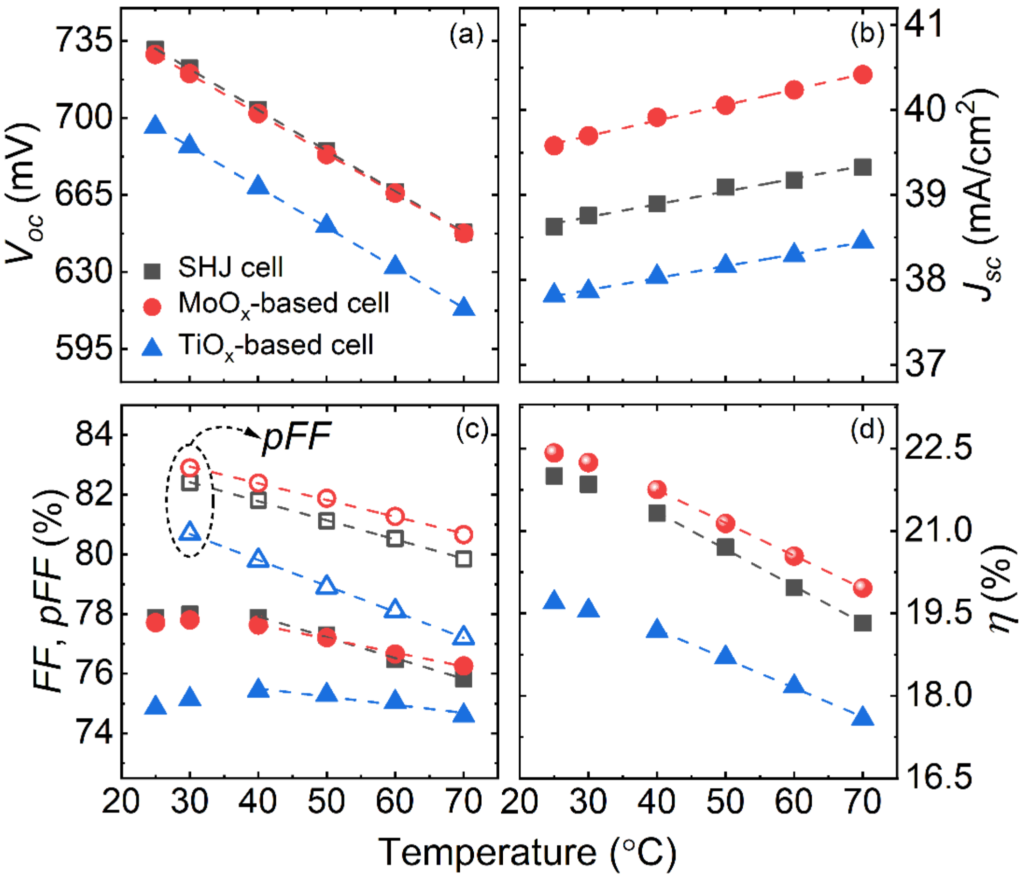

Figure 2: Cell parameters of the standard SHJ, MoO_x-, and TiO_x-based solar cells including (a) V_{oc}, (b) J_{sc}, (c) *FF* and *pFF* (open symbols), and (d) η under one-sun illumination as a function of temperature.

The extracted TCs are summarized in Table 1. The TC_{FF} and TC_{η} of all the investigated cells are extracted from linear fits in the temperature range from 40 to 70 °C (the linear range). The *FF* and η at 25 °C are then obtained by extrapolation to determine relative TCs. The TCs obtained in this study are compared to those of other cell structures reported in Refs. [2, 19] and presented in Figs. 3(a)-(d).

Table 1: Extracted TCs and the gamma factor (γ), as well as their statistical errors determined from the standard deviation of the linear regression, for the standard SHJ, MoO_x- and TiO_x-based solar cells.

	TC_{Voc} (%/°C)	TC_{Jsc} (%/°C)	TC_{FF} (%/°C)	TC_{pFF} (%/°C)	TC_{η} (%/°C)	γ
SHJ cell	−0.254±0.001	+0.039±0.002	−0.088±0.004	−0.077±0.001	−0.301±0.007	3
MoO_x-based cell	−0.248±0.001	+0.046±0.001	−0.059±0.003	−0.067±0.002	−0.264±0.003	2.4
TiO_x-based cell	−0.264±0.001	+0.037±0.001	−0.036±0.006	−0.107±0.001	−0.265±0.008	1.4

Focusing on TC_{Voc}, it is well known that the temperature sensitivity of V_{oc} of a Si solar cell depends on both V_{oc} and gamma factor (γ), as described in the following equation [5]:

$$TC_{Voc} = \frac{dV_{oc}}{dT} = -\frac{E_{g0}/q - V_{oc} + \gamma k_B T/q}{T} \quad (1)$$

where E_{g0} is the semiconductor bandgap linearly extrapolated to 0 K, q is the elementary charge, k_B is the Boltzmann constant, and T is the temperature. γ represents the temperature dependence of the diode saturation current density in the solar cells, and hence, it contains information about the dominant recombination mechanism [1, 54]. The extracted values for γ using Eq. 1 are summarised in Table 1. Here we use E_{g0} = 1.206 eV for all the calculations of the studied cells due to their similar wafer resistivity [55]. The different γ values explain the slightly superior TC_{Voc} of the MoO_x-based cell to that of the standard SHJ cell, despite a negligible difference between the initial V_{oc} of the two cell structures [731.2 mV (standard SHJ) and 728.9 mV (MoO_x-based) at 25 °C]. The inferior TC_{Voc} of the TiO_x-based cell is expected as its initial V_{oc} is lower than those of the standard SHJ and MoO_x-based cells. For this cell structure, this effect is being dominant over the impact of the γ.

Compared to the TC_{Voc} of other cell structures as shown in Fig. 3(a), the obtained TC_{Voc} of the MoO_x-based solar cell is comparable to that of the SHJ cells while the TiO_x-based cell's TC_{Voc} is almost identical to the TOPCon cells' TC_{Voc}. The TC_{Voc} of both MoO_x- and TiO_x-based cells are superior to those of the cells without passivating contacts [advanced passivated emitter rear totally diffused (adv. PERT), PERT, passivated emitter and rear contact (PERC), and aluminium back surface field (Al-BSF) cells]. Battaglia *et al.* [46] and Sacchetto *et al.* [53] reported that the decreasing trend of V_{oc} of the MoO_x-based cells is less pronounced compared to that of the SHJ cells as a function of temperature. This implies a superior TC_{Voc} of the MoO_x-based cells, agreeing with our findings.

The TC_{Jsc} of the TiO_x-based solar cell is comparable to that of the standard SHJ cell, whereas the TC_{Jsc} of the MoO_x-based cell is more favourable than those of the former two cells. The spectral response of the studied cells at different temperatures will be presented and discussed in Section 3.5 to clarify this trend. The TC_{Jsc} of the MoO_x-based cell is comparable to that of the TOPCon cell and better than those of all the others, except for the Al-BSF cell (the superior TC_{Jsc} of the Al-BSF cell is discussed in Ref. [19]). Meanwhile, the TC_{Jsc} of the SHJ and TiO_x-based cells are comparable to those of the advanced PERT, PERT, and PERC cells.

The TC_{FF} of the MoO_x- and TiO_x-based solar cells are superior to those of any other cell, including the SHJ. Furthermore, their TC_{FF} are better than their TC_{pFF}, whereas the standard SHJ cell shows an opposite trend. This indicates that R_s of the two former cells reduces at elevated temperatures while the latter cell's R_s increases. The temperature-dependent behaviour of R_s of the investigated cells will be discussed in Section 3.3. To quantify the contribution of V_{oc} and R_s to TC_{FF} of the studied cells, the following equations are used [56, 57]:

$$\frac{1}{FF}\frac{dFF}{dT} = (1-1.02FF_0)\left(\frac{1}{V_{oc}}\frac{dV_{oc}}{dT} - \frac{1}{T}\right) - \frac{R_s}{V_{oc}/I_{sc} - R_s}\left(\frac{1}{R_s}\frac{dR_s}{dT}\right) \quad (2)$$

where

$$FF_0 = \frac{\nu_{oc} - \ln(\nu_{oc}+0.72)}{\nu_{oc}+1} \quad (3)$$

where FF_0 is the ideal FF, in the absence of R_s and shunt resistance (R_{sh}) effects. ν_{oc} is the normalized V_{oc} to the thermal voltage (nkT/q). The first term in Eq. (2) represents the contribution of V_{oc} to TC_{FF} while the second term indicates the contribution of R_s to the TC_{FF}. For the cell structures studied here, the contribution of V_{oc} to TC_{FF} is dominant and accounts for more than 60%; indicating that the temperature-dependent behaviour of FF strongly depends on the increase of $n_{i,eff}$ at elevated temperatures caused by bandgap narrowing [41]. It is noteworthy that the contribution of R_s to TC_{FF} is considerably more significant for the TiO_x-based cell (nearly 36%) than for the other two cell structures. It offsets the decrease of the TiO_x-based cell's V_{oc} at elevated temperature, resulting in a greatly superior TC_{FF} of this cell.

The TC_η of the MoO_x- and TiO_x-based solar cells are almost identical. They are better than that of the standard SHJ cell and greatly superior to those of other cell structures reported in the literature. The obtained TC_η highlight the advantage of using TMO-integrated cells in the field. As expected, the contribution of TC_{Voc} to TC_η is dominant and accounts for more than 60% for all the cell structures shown in Fig. 3. Battaglia *et al.* [46] and Sacchetto *et al.* [53] also reported that the decreasing trend of the MoO_x-based cells' efficiency is less pronounced compared to that of the SHJ cells' efficiency as a function of temperature. This implies a favourable TC_η of the MoO_x-based cells in agreement with our findings.

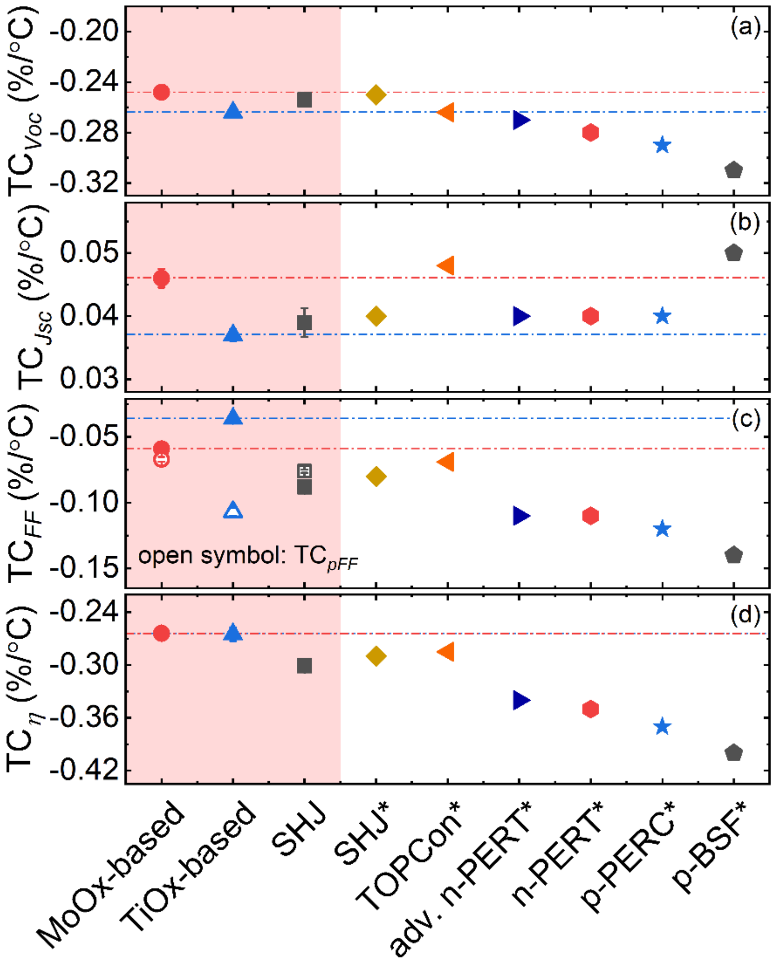

Figure 3: (a) TC_{Voc}, (b) TC_{Jsc}, (c) TC_{FF} and TC_{pFF}, and (d) TC_η of the standard SHJ, MoO_x- and TiO_x-based solar cells extracted from the slopes of linear fits of the cell parameters as a function of temperature as shown in Fig. 2. Error bars are obtained from the linear fits. TCs of solar cell structures reported in the literature [2, 19] (axis labels with star mark) are also shown for comparison.

3.2. Temperature and illumination intensity dependence of solar cells

In Section 3.1, we discussed the temperature sensitivity of the cell parameters at one-sun. However, in the field, solar cells do not only operate at different temperatures, but they are also exposed to a large range of illumination intensities. Since TC_{Voc} dominates the TC_{η} for all the studied cells, it can indicate the temperature sensitivity of the cells at different intensities.

Suns-V_{oc} measurements of the investigated cells in the temperature range from 30 to 80 °C are presented in Figs. 4(a)-(c). For all three cell structures, a significant reduction of V_{oc} at low illumination intensities can be seen. This reduction is less pronounced at higher illumination intensities. TC_{Voc} of the studied cells extracted from Suns-V_{oc} measurements (open symbols) as a function of illumination intensity is presented in Fig. 4(d). TC_{Voc} obtained from *I-V* measurements (solid symbols) at one sun illumination are also shown for comparison. We find that the TC_{Voc} at one sun illumination extracted from both measurement methods match well (in the range of 1.2%). For all the cells, the absolute value of TC_{Voc} decreases with increasing illumination intensity (less negative); indicating that the studied cells are less sensitive to temperature variation at higher illumination intensities. It is noteworthy that the TC_{Voc} of the MoO_x-based and SHJ cells similarly behave as a function of illumination intensity while the illumination intensity dependence of TC_{Voc} is more pronounced for the TiO_x-based cell. For most of the intensity range, this observation can be attributed to the lower initial V_{oc} of the TiO_x-based cell (as obtained from the Suns-V_{oc} measurements; not shown here) compared to the initial V_{oc} of the other cells. However, at high illumination intensities (> 3 suns), it seems the γ has a significant impact on the TC_{Voc} of the TiO_x-based cell.

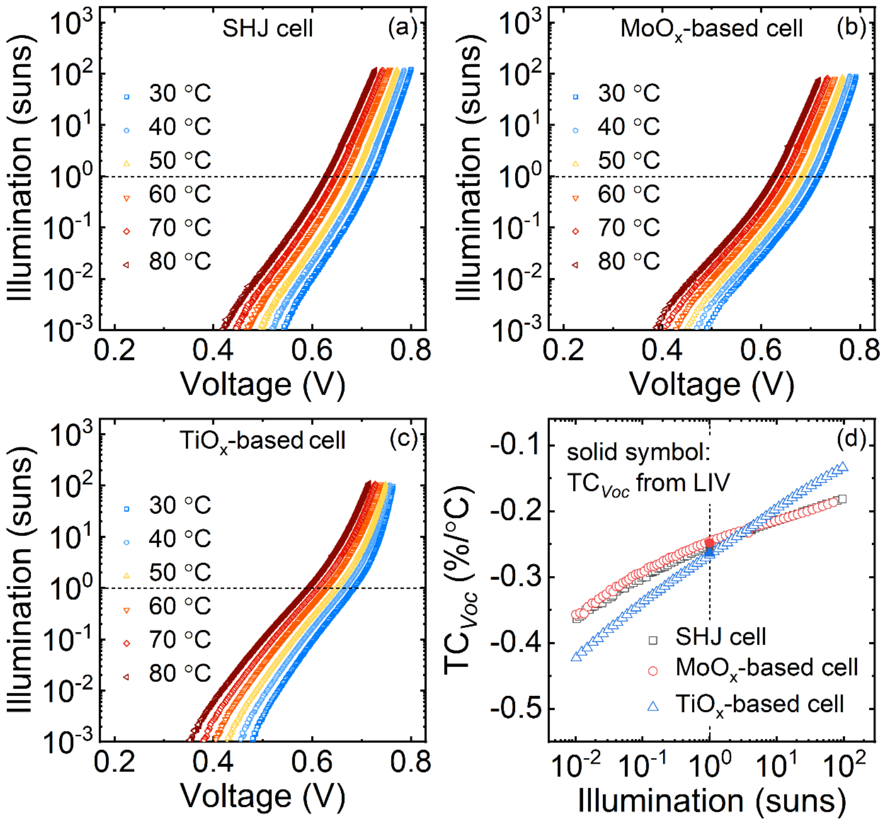

Figure 4: Suns-V_{oc} measurements of (a) the standard SHJ, (b) MoO_x-, and (c) TiO_x-based solar cells at different temperatures. (d) TC_{Voc} extracted from Suns-V_{oc} (open symbols) and *I-V* (solid symbols) measurements as a function of illumination intensity.

3.3. Temperature dependence of R_s

Figure 3(c) highlights the superiority of TMO-based solar cells in regard to TC_{FF}. As mentioned, we expected that R_s of the MoO_x- and TiO_x-based solar cells reduce at elevated temperatures, whereas the standard SHJ cell's R_s increases. This section investigates the temperate dependence of the studied cells' R_s and several components that contributes to R_s to explain the findings.

R_s of the studied cells as a function of temperature are shown in Fig. 5. Indeed, R_s of the MoO_x- and TiO_x-based solar cells reduce with increasing temperature while the standard SHJ cell's R_s increases. As expected from the difference between TC_{FF} and TC_{pFF} of these cells [see Fig. 3(c)], the reduction of the TiO_x-based cell's R_s at elevated temperatures is more pronounced compared to that of the MoO_x-based cell's R_s. The extracted TC_{Rs} of the studied solar cells are summarized in Table 2. Note that the R_{sh} of these cells, as determined from the linear fit of the *I*-*V* measurement around $V = 0$ V (not shown here), are extremely large (in the range of 10k-30k $\Omega{\cdot}cm^2$). They are therefore assumed not to impact the temperature dependence of *FF*.

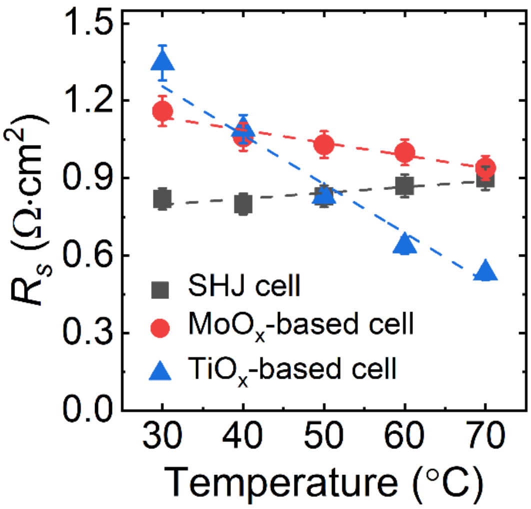

Figure 5: R_s of the standard SHJ, MoO_x-, and TiO_x-based solar cells as a function of temperature.

Table 2: Extracted TC_{Rs} and their statistical errors of the linear regression determined from the standard deviation for the standard SHJ, MoO_x- and TiO_x-based solar cells.

	Standard SHJ cell	MoO_x-based cell	TiO_x-based cell
TC_{Rs} (%/°C)	+0.281±0.082	−0.414±0.057	−1.314±0.149

R_s of the studied cells consists of the contributions of the rear metal contact, the electron-collector ($R_{e\text{-}col(r)}$), the Si wafer, the hole-collector ($R_{h\text{-}col(f)}$), the lateral transport within the front ITO layer, the interfacial contact between the front ITO layer and the front metal contacts, and the front metal contacts including fingers and busbars. $R_{e\text{-}col(r)}$ and $R_{h\text{-}col(f)}$ can be obtained from the ρ_c test structures. Since the temperature of the curing process after metallization is different for the investigated solar cells (see Section 2.1), the possibility that the impact of this process on the contribution of components to the cells' R_s is varied might not be excluded. Note that the $R_{e\text{-}col(r)}$ and $R_{h\text{-}col(f)}$ obtained from the ρ_c test structures represent their upper limit. They will be presented in the next sections.

3.3.1 Temperature dependence of contact resistivity of the hole-collector

To gain a deeper understanding regarding the difference between the standard SHJ and MoO_x-based cells, the a-Si:H(i/p)- and MoO_x-based test structures are studied. Figure 6 presents ρ_c obtained from these structures as a function of temperature. Interestingly, the temperature dependence of ρ_c shows opposite trends. When the temperature increases from 25 to 80 °C, the ρ_c of the a-Si:H(i/p)-based structures increases from 0.17 to 0.23 $\Omega \cdot cm^2$, whereas the ρ_c of the MoO_x-based structures decreases from 0.32 to 0.17 $\Omega \cdot cm^2$. The carrier transport via thermionic barrier is usually improved at elevated temperatures [51]. Therefore, the significant decrease of ρ_c of the MoO_x-based structures may indicate a large thermionic component in the carrier transport across the contact. Meanwhile, the ρ_c increase of the a-Si:H(i/p)-based structures may imply that the carrier transport via thermionic barrier in this contact becomes less pronounced. It is noteworthy that the rate of change of the ρ_c against temperature for the two test structures is lower than that of the R_s for these corresponding cells, indicating that other components also contribute to the temperature-dependent behaviour of their *FF*. It seems that the improvement of ρ_c of the MoO_x-based structures at elevated temperatures counterbalances some of the *FF* losses, resulting in a less temperature-sensitive *FF*.

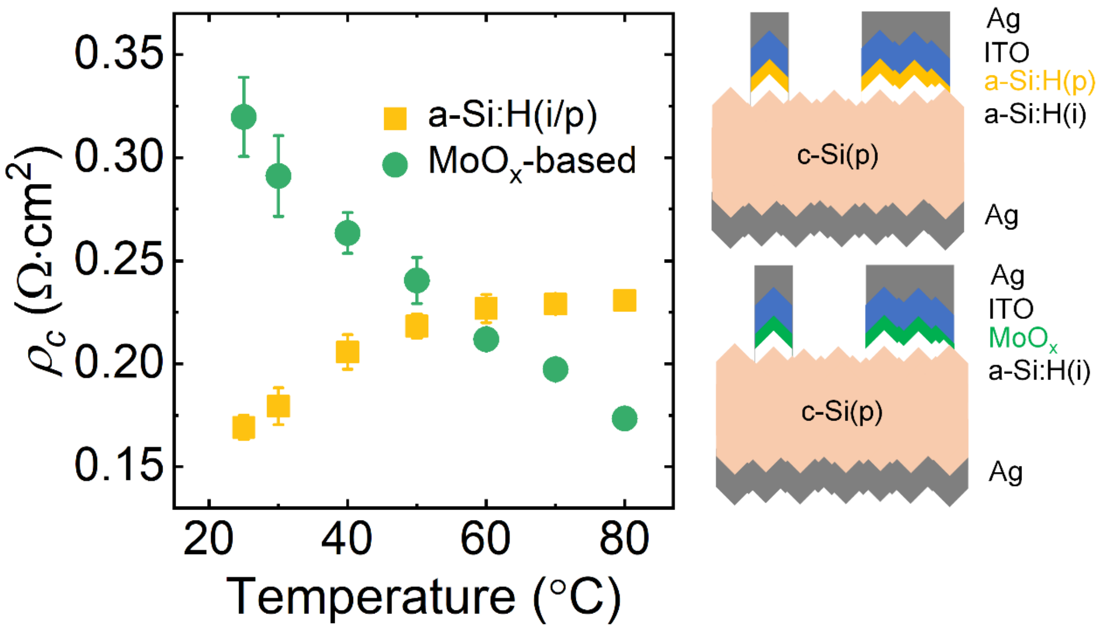

Figure 6: ρ_c of the a-Si:H(i/p)- and MoO_x-based test structures as a function of temperature. Sketches of the Cox and Strack test structures are shown next to the figure.

3.3.2 Temperature dependence of contact resistivity of the electron-collector

To compare between the standard SHJ and TiO_x-based cells, the a-Si:H(i/n)- and TiO_x-based test structures are investigated. Figure 7 presents ρ_c obtained from these structures as a function of temperature. Again, an opposite trend is observed. When the temperature increases from 25 to 80 °C, the ρ_c of the a-Si:H(i/n)-based structures increases from 0.10 to 0.15 $\Omega \cdot cm^2$, whereas the ρ_c of the TiO_x-based structures decreases from 0.68 to 0.04 $\Omega \cdot cm^2$. As in the previous section, a large thermionic component in the carrier transport can explain the significant decrease of ρ_c of the TiO_x-based structures [51]. We also find that the rate of change of the ρ_c against temperature for the two test structures is lower than that of the two corresponding cells' R_s. Similar to the MoO_x-based structures, the improvement of ρ_c of the TiO_x-based structures with increasing temperature counterbalances some of the *FF* losses of this cell, resulting in its favourable TC_{FF}.

Compared to the a-Si:H(i/p)-based test structures, the ρ_c of the a-Si:H(i/n)-based test structures is lower at any given temperature as shown in the inset of Fig. 7. This phenomenon was also reported in Ref. [51] and can be explained by the usually much smaller conduction band offset in the a-Si:H(i/n)-based structure compared to the valence band offset in the a-Si:H(i/p)-based structures [58]. Thus, the hole transport is impeded by the a-Si:H(i) layer [58]. The extracted ρ_c of both a-Si:H(i/n)- and TiO-based test structures are comparable to those previously reported [47, 51].

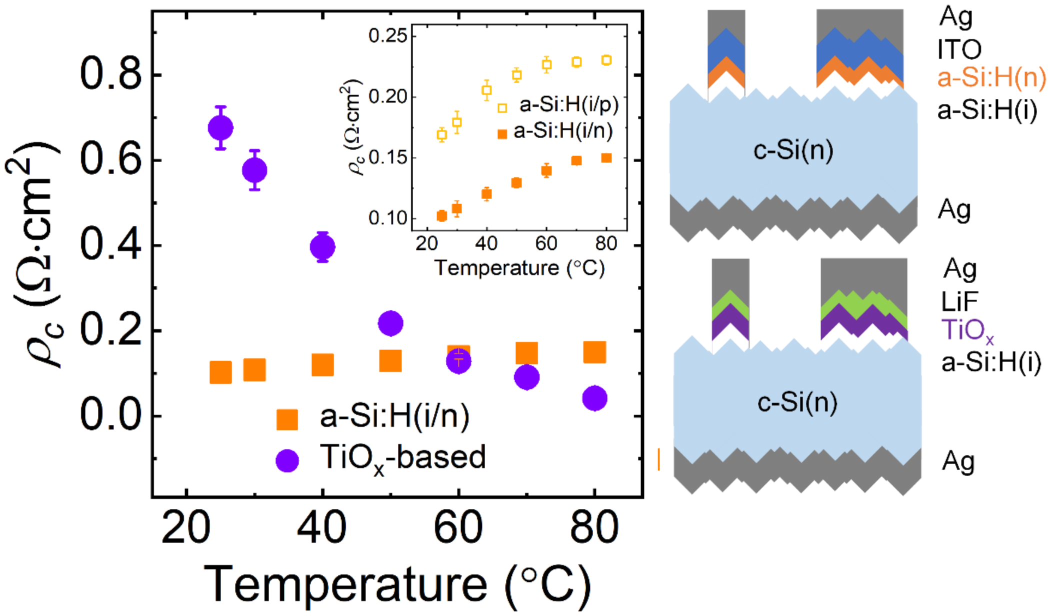

Figure 7: ρ_c of the a-Si:H(i/n)- and TiO_x-based test structures as a function of temperature. Sketches of the Cox and Strack test structures are shown next to the figure. The inset compares ρ_c of the a-Si:H(i/p)- (open symbols) and a-Si:H(i/n)-based (solid symbols) test structures.

3.4. Temperature dependence of surface passivation

In this section, we investigate the temperature-dependent behaviour of J_{0s}, one of the key parameters indicating the quality of a passivating contact. The extracted J_{0s} using lifetime measurements on the symmetrical test structures as a function of temperature are depicted Figs. 8(a)-(b). We observe a significant increase of J_{0s}, which is due to the increase of $n_{i,eff}$ caused by bandgap narrowing [41], since J_{0s} is proportional to $n_{i,eff}^2$ [59]. More meaningful information is obtained from the $J_{0s}/n_{i,eff}^2$ ratio as a function of temperature. If the gain of J_{0s} at elevated temperatures is solely determined by $n_{i,eff}$, the ratio needs to be temperature independent. As a reduction of the ratios with increasing temperature is observed regardless of the test structures, an improvement of the passivation quality at elevated temperature can be assumed. This improvement is more pronounced for the MoO_x-based lifetime test structures compared to the other structures. TCs of the $J_{0s}/n_{i,eff}^2$ ratio are extracted and summarized in Table 3. This improvement can result in a better response of the EQE spectrum of the MoO_x-based cell at the short wavelength region, as will be discussed in the next section. Nevertheless, it seems that the improvement of the passivation quality observed for all the lifetime test structures does not have a strong impact on TC_{Voc} of the investigated solar cells.

Table 3: Extracted TCs of the $J_{0s}/n_{i,eff}^2$ ratio and their statistical errors determined from the standard deviation of the linear regression for the standard SHJ, MoO_x- and TiO_x-based solar cells.

	a-Si:H(i/p)	MoO_x-based	a-Si:H(i/n)	TiO_x-based
$TC_{J0s/ni,eff2}$ (%/°C)	−0.56±0.02	−0.90±0.03	−0.46±0.05	−0.47±0.05

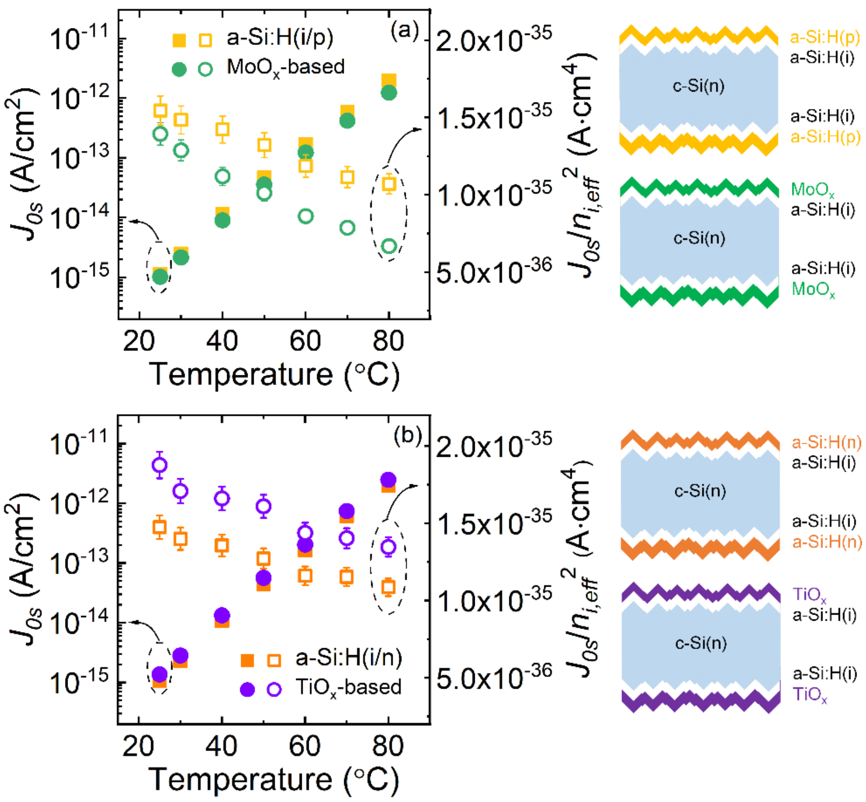

Figure 8: J_{0s} and $J_{0s}/n_{i,eff}^2$ ratios of (a) the a-Si:H(i/p)- and MoO_x-based, (b) the a-Si:H(i/n)- and TiO_x-based lifetime test structures as a function of temperature. Sketches of the symmetrical lifetime test structures used in this study are shown next to the figures.

3.5. Temperature dependence of EQE

As discussed in Section 3.1, the TC_{Jsc} of the TiO_x-based solar cell is comparable to that of the standard SHJ cell, whereas the TC_{Jsc} of the MoO_x-based cell is superior to those of the former two cell structures. In this section, we investigate the temperature-dependent EQE of the studied solar cells to explain these findings.

The EQE measurements of the studied solar cells at 25 °C and 45 °C in the wavelength ranges of 300-600 nm (short wavelengths) and 900-1200 nm (long wavelengths) are presented in Figs. 9(a)-(b), respectively. For the short wavelength region, the EQE at the two temperatures are almost identical for the standard SHJ and TiO_x-based cells, whereas a slight increase is observed for the MoO_x-based cell. For the long wavelength region, the spectral response is improved with increasing temperature, regardless of the cell structures. This improvement is attributed to bandgap narrowing of the Si at elevated temperatures [1, 60] that has a critical impact on this wavelength range.

The gain of J_{sc} between 25 °C and 45 °C determined from the EQE, split into different wavelength ranges, is presented in Fig. 9(c). The J_{sc} of the MoO_x-based cell gains 0.36 mA/cm^2, 0.05-0.06 mA/cm^2 higher than the J_{sc} gain of the other two cells. The J_{sc} gains in the wavelength ranges of 600-900 nm and 900-1200 nm are almost identical for all the cells, whereas the J_{sc} gain in the wavelength range of 300-600 nm is different. Based on Section 3.4, the better spectral response at the short wavelengths for the MoO_x-based cell can be attributed to the larger improvement of the passivation quality of the MoO_x-based passivating contacts with increasing temperature. To strengthen this point, we established a model using the AFORS-HET simulation tool [61] and successfully reproduce the trend of the spectral response at the short wavelength region by modifying the ratio between the electron and hole capture cross sections (σ_n/σ_p), as shown in Fig. 2S. Hence, the favourable TC_{Jsc} of the MoO_x-based cell can be explained by the large improvement of the passivation quality of the MoO_x-based passivating contacts, resulted in the increase of the spectral response at elevated temperatures in the short wavelength range.

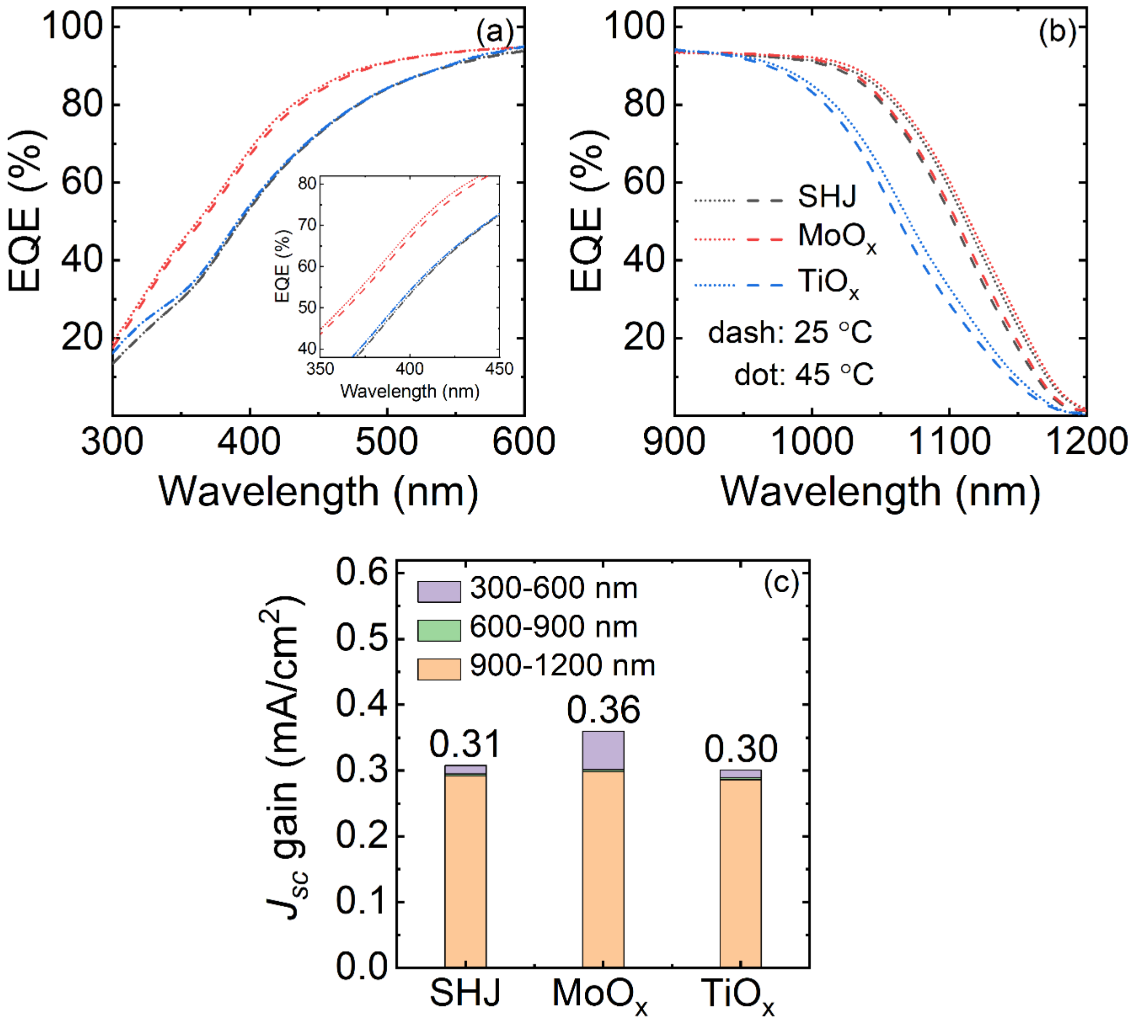

Figure 9: EQE measurements of the standard SHJ, MoO_x-, and TiO_x-based solar cells at 25 °C and 45 °C in the range of wavelength (a) from 300 to 600 nm, and (b) from 900 to 1200 nm. (c) J_{sc} gain between 25 °C and 45 °C at different wavelength regions.

4. Conclusion

The temperature-dependent performance of TMO-based passivating contacts and their devices was investigated. The TC_η of the MoO_x- and TiO_x-based solar cells are almost identical. They are better than that of the standard SHJ cell, and greatly superior to those of the cell structures without passivating contacts. The findings highlight the advantage of using solar cells that integrate TMO-based passivating contacts in the field.

The superior TC_η of the MoO_x-based cell is mainly due to the favourable TC_{Jsc} and TC_{FF} while the TC_η superiority of the TiO_x-based cell is solely from a superior TC_{FF}. The favourable TC_{Jsc} of the MoO_x-based cell compared to the other two cell structures can be explained by a better spectral response at the short wavelength region with increasing temperature, resulting from an improvement in the passivation quality of the MoO_x-based passivating contacts. The superior TC_{FF} of the MoO_x- and TiO_x-based solar cells are partly contributed by the improvement of ρ_c of their passivating contacts at elevated temperatures which counterbalances some of the *FF* losses, resulting in a less temperature-sensitive *FF*.

Furthermore, it was concluded that the studied cells are less sensitive to temperature variation at higher illumination intensities. The TC_{Voc} of the MoO_x-based and SHJ cells behave the same as a function of illumination intensity while the illumination intensity dependence is more pronounced for the TiO_x-based cell.

Acknowledgement

This work was supported by the Australian Government through Australian Renewable Energy Agency [ARENA; project 2017/RND001]. The views expressed herein are not necessarily the views of the Australian Government, and the Australian Government does not accept responsibility for any information or advice contained herein.

References

[1] O. Dupré, R. Vaillon, M.A. Green, Thermal behavior of photovoltaic devices, Springer, Switzerland, 2017.
[2] J. Haschke, J.P. Seif, Y. Riesen, A. Tomasi, J. Cattin, L. Tous, P. Choulat, M. Aleman, E. Cornagliotti, A. Uruena, R. Russell, F. Duerinckx, J. Champliaud, J. Levrat, A.A. Abdallah, B. Aissa, N. Tabet, N. Wyrsch, M. Despeisse, J. Szlufcik, S. De Wolf, C. Ballif, The impact of silicon solar cell architecture and cell interconnection on energy yield in hot & sunny climates, Energ Environ Sci, 10 (2017) 1196–1206.
[3] M. Kasu, J. Abdu, S. Hara, S. Choi, Y. Chiba, A. Masuda, Temperature dependence measurements and performance analyses of high-efficiency interdigitated back-contact, passivated emitter and rear cell, and silicon heterojunction photovoltaic modules, Japanese Journal of Applied Physics, 57 (2018) 08RG18.
[4] P. Singh, N.M. Ravindra, Temperature dependence of solar cell performance—an analysis, Sol Energ Mat Sol C, 101 (2012) 36-45.
[5] M.A. Green, General temperature dependence of solar cell performance and implications for device modelling, Progress in Photovoltaics: Research and Applications, 11 (2003) 333–340.
[6] F. Haase, C. Hollemann, S. Schafer, A. Merkle, M. Rienacker, J. Krugener, R. Brendel, R. Peibst, Laser contact openings for local poly-Si-metal contacts enabling 26.1%-efficient POLO-IBC solar cells, Sol Energ Mat Sol C, 186 (2018) 184–193.
[7] N. Nandakumar, J. Rodriguez, T. Kluge, T. Grosse, L. Fondop, P. Padhamnath, N. Balaji, M. Konig, S. Duttagupta, Approaching 23% with large-area monoPoly cells using screen-printed and fired rear passivating contacts fabricated by inline PECVD, Progress in Photovoltaics: Research and Applications, 27 (2019) 107–112.
[8] K. Yoshikawa, H. Kawasaki, W. Yoshida, T. Irie, K. Konishi, K. Nakano, T. Uto, D. Adachi, M. Kanematsu, H. Uzu, Silicon heterojunction solar cell with interdigitated back contacts for a photoconversion efficiency over 26%, Nat Energy, 2 (2017) 17032.
[9] A. Richter, J. Benick, F. Feldmann, A. Fell, M. Hermle, S.W. Glunz, n-Type Si solar cells with passivating electron contact: Identifying sources for efficiency limitations by wafer thickness and resistivity variation, Sol Energ Mat Sol C, 173 (2017) 96-105.
[10] J. Bullock, Y. Wan, M. Hettick, X. Zhaoran, S.P. Phang, D. Yan, H. Wang, W. Ji, C. Samundsett, Z. Hameiri, Dopant-free partial rear contacts enabling 23% silicon solar cells, Adv Energy Mater, 9 (2019) 1803367.
[11] J. Dréon, Q. Jeangros, J. Cattin, J. Haschke, L. Antognini, C. Ballif, M. Boccard, 23.5%-efficient silicon heterojunction silicon solar cell using molybdenum oxide as hole-selective contact, Nano Energy, 70 (2020) 104495.

[12] A. Cuevas, Y.M. Wan, D. Yan, C. Samundsett, T. Allen, X.Y. Zhang, J. Cui, J. Bullock, Carrier population control and surface passivation in solar cells, Sol Energ Mat Sol C, 184 (2018) 38–47.
[13] T.G. Allen, J. Bullock, X. Yang, A. Javey, S. De Wolf, Passivating contacts for crystalline silicon solar cells, Nat Energy, (2019) 1-15.
[14] J. Melskens, B.W.H. van de Loo, B. Macco, L.E. Black, S. Smit, W.M.M. Kessels, Passivating contacts for crystalline silicon solar cells: From concepts and materials to prospects, IEEE J Photovolt, 8 (2018) 373–388.
[15] D. Adachi, J.L. Hernández, K. Yamamoto, Impact of carrier recombination on fill factor for large area heterojunction crystalline silicon solar cell with 25.1% efficiency, Appl Phys Lett, 107 (2015) 233506.
[16] K. Masuko, M. Shigematsu, T. Hashiguchi, D. Fujishima, M. Kai, N. Yoshimura, T. Yamaguchi, Y. Ichihashi, T. Mishima, N. Matsubara, Achievement of more than 25% conversion efficiency with crystalline silicon heterojunction solar cell, IEEE J Photovolt, 4 (2014) 1433-1435.
[17] K. Yoshikawa, H. Kawasaki, W. Yoshida, T. Irie, K. Konishi, K. Nakano, T. Uto, D. Adachi, M. Kanematsu, H. Uzu, Silicon heterojunction solar cell with interdigitated back contacts for a photoconversion efficiency over 26%, Nat Energy, 2 (2017) 1-8.
[18] F. Haase, C. Hollemann, S. Schäfer, A. Merkle, M. Rienäcker, J. Krügener, R. Brendel, R. Peibst, Laser contact openings for local poly-Si-metal contacts enabling 26.1%-efficient POLO-IBC solar cells, Sol Energ Mat Sol C, 186 (2018) 184-193.
[19] A.H.T. Le, R. Basnet, D. Yan, W. Chen, N. Nandakumar, S. Duttagupta, J.P. Seif, Z. Hameiri, Temperature-dependent performance of silicon solar cells with polysilicon passivating contacts, Sol Energ Mat Sol C, 225 (2021) 111020.
[20] A.H.T. Le, R. Basnet, D. Yan, W. Chen, J.P. Seif, Z. Hameiri, Temperature dependence of polysilicon passivating contact and its device performance, 47th IEEE Photovoltaic Specialists Conference, (2020) 1020-1023.
[21] J. Bullock, D. Yan, A. Cuevas, Y. Wan, C. Samundsett, n-and p-typesilicon solar cells with molybdenum oxide hole contacts, Energy Procedia, 77 (2015) 446-450.
[22] L.G. Gerling, S. Mahato, A. Morales-Vilches, G. Masmitja, P. Ortega, C. Voz, R. Alcubilla, J. Puigdollers, Transition metal oxides as hole-selective contacts in silicon heterojunctions solar cells, Sol Energ Mat Sol C, 145 (2016) 109-115.
[23] X. Yang, H. Xu, W. Liu, Q. Bi, L. Xu, J. Kang, M.N. Hedhili, B. Sun, X. Zhang, S. De Wolf, Atomic layer deposition of vanadium oxide as hole-selective contact for crystalline silicon solar cells, Advanced Electronic Materials, 6 (2020) 2000467.
[24] S. Essig, J. Dréon, J. Werner, P. Löper, S. De Wolf, M. Boccard, C. Ballif, MoO_x and WO_x based hole-selective contacts for wafer-based Si solar cells, in: 2017 IEEE 44th Photovoltaic Specialist Conference (PVSC), IEEE, 2017, pp. 55-58.
[25] W. Wang, J. He, D. Yan, C. Samundsett, S.P. Phang, Z. Huang, W. Shen, J. Bullock, Y. Wan, 21.3%-efficient n-type silicon solar cell with a full area rear TiO_x/LiF/Al electron-selective contact, Sol Energ Mat Sol C, 206 (2020) 110291.
[26] Y.M. Wan, C. Samundsett, J. Bullock, M. Hettick, T. Allen, D. Yan, J. Peng, Y.L. Wu, J. Cui, A. Javey, A. Cuevas, Conductive and stable magnesium oxide electron-selective contacts for efficient silicon solar cells, Adv Energy Mater, 7 (2017) 1601863.
[27] J. Bullock, Y. Wan, Z. Xu, S. Essig, M. Hettick, H. Wang, W. Ji, M. Boccard, A. Cuevas, C. Ballif, Stable dopant-free asymmetric heterocontact silicon solar cells with efficiencies above 20%, ACS Energy Letters, 3 (2018) 508-513.
[28] J. Geissbühler, J. Werner, S. Martin de Nicolas, L. Barraud, A. Hessler-Wyser, M. Despeisse, S. Nicolay, A. Tomasi, B. Niesen, S. De Wolf, 22.5% efficient silicon heterojunction solar cell with molybdenum oxide hole collector, Appl Phys Lett, 107 (2015) 081601.
[29] W. Wu, W. Lin, S. Zhong, B. Paviet-Salomon, M. Despeisse, Z. Liang, M. Boccard, H. Shen, C. Ballif, 22% efficient dopant-free interdigitated back contact silicon solar cells, in: AIP Conference Proceedings, AIP Publishing LLC, 2018, pp. 040025.
[30] W. Kern, The evolution of silicon-wafer cleaning technology, J Electrochem Soc, 137 (1990) 1887–1892.

[31] R.H. Cox, H. Strack, Ohmic contacts for GaAs devices, Solid State Electron, 10 (1967) 1213–1218.
[32] A.H.T. Le, R. Basnet, D. Yan, W. Chen, J.P. Seif, Z. Hameiri, Temperature dependence of polysilicon passivating contact and its device performance, in: 47th IEEE Photovoltaic Specialists Conference, IEEE, 2020, pp. 1020-1023.
[33] M. Wolf, H. Rauschenbach, Series resistance effects on solar cell measurements, Advanced energy conversion, 3 (1963) 455-479.
[34] Y. Zhu, F. Rougieux, N.E. Grant, J.A.T. De Guzman, J.D. Murphy, V.P. Markevich, G. Coletti, A.R. Peaker, Z. Hameiri, Electrical characterization of thermally activated defects in n-type float-zone silicon, IEEE J Photovolt, 11 (2020) 26-35.
[35] A. Fell, A free and fast three-dimensional/two-dimensional solar cell simulator featuring conductive boundary and quasi-neutrality approximations, IEEE T Electron Dev, 60 (2013) 733–738.
[36] R. Dumbrell, M.K. Juhl, T. Trupke, Z. Hameiri, Extracting metal contact recombination parameters from effective lifetime data, 8 (2018) 1413-1420.
[37] K.R. McIntosh, R.A. Sinton, Uncertainty in photoconductance lifetime measurements that use an inductive-coil detector, in: 23rd European Photovoltaic Solar Energy Conference, 2008, pp. 77-82.
[38] A. Schenk, Finite-temperature full random-phase approximation model of band gap narrowing for silicon device simulation, J Appl Phys, 84 (1998) 3684–3695.
[39] A. Richter, S.W. Glunz, F. Werner, J. Schmidt, A. Cuevas, Improved quantitative description of Auger recombination in crystalline silicon, Phys Rev B, 86 (2012) 165202.
[40] D.B.M. Klaassen, A unified mobility model for device simulation—I. Model-equations and concentration-dependence, Solid State Electron, 35 (1992) 953–959.
[41] R. Pässler, Semi-empirical descriptions of temperature dependences of band gaps in semiconductors, physica status solidi (b), 236 (2003) 710-728.
[42] W. van Sark, L. Korte, F. Roca, Physics and technology of amorphous-crystalline heterostructure silicon solar cells, Springer, 2012.
[43] M. Bivour, J. Temmler, H. Steinkemper, M. Hermle, Molybdenum and tungsten oxide: High work function wide band gap contact materials for hole selective contacts of silicon solar cells, Sol Energ Mat Sol C, 142 (2015) 34-41.
[44] J. Meyer, S. Hamwi, M. Kröger, W. Kowalsky, T. Riedl, A. Kahn, Transition metal oxides for organic electronics: Energetics, device physics and applications, Advanced materials, 24 (2012) 5408-5427.
[45] M.T. Greiner, M.G. Helander, W.-M. Tang, Z.-B. Wang, J. Qiu, Z.-H. Lu, Universal energy-level alignment of molecules on metal oxides, Nature materials, 11 (2012) 76-81.
[46] C. Battaglia, S.M. De Nicolas, S. De Wolf, X. Yin, M. Zheng, C. Ballif, A. Javey, Silicon heterojunction solar cell with passivated hole selective MoO_x contact, Appl Phys Lett, 104 (2014) 113902.
[47] J. Bullock, M. Hettick, J. Geissbühler, A.J. Ong, T. Allen, C.M. Sutter-Fella, T. Chen, H. Ota, E.W. Schaler, S. De Wolf, Efficient silicon solar cells with dopant-free asymmetric heterocontacts, Nat Energy, 1 (2016) 1-7.
[48] Z.C. Holman, S. De Wolf, C. Ballif, Improving metal reflectors by suppressing surface plasmon polaritons: a priori calculation of the internal reflectance of a solar cell, Light: Science & Applications, 2 (2013) e106-e106.
[49] Z.C. Holman, M. Filipič, B. Lipovšek, S. De Wolf, F. Smole, M. Topič, C. Ballif, Parasitic absorption in the rear reflector of a silicon solar cell: Simulation and measurement of the sub-bandgap reflectance for common dielectric/metal reflectors, Sol Energ Mat Sol C, 120 (2014) 426-430.
[50] M. Taguchi, E. Maruyama, M. Tanaka, Temperature dependence of amorphous/crystalline silicon heterojunction solar cells, Japanese Journal of Applied Physics, 47 (2008) 814.
[51] G. Nogay, J.P. Seif, Y. Riesen, A. Tomasi, Q. Jeangros, N. Wyrsch, F.-J. Haug, S. De Wolf, C. Ballif, Nanocrystalline silicon carrier collectors for silicon heterojunction solar cells and impact on low-temperature device characteristics, IEEE J Photovolt, 6 (2016) 1654-1662.

[52] J.P. Seif, D. Menda, A. Descoeudres, L. Barraud, O. Özdemir, C. Ballif, S. De Wolf, Asymmetric band offsets in silicon heterojunction solar cells: Impact on device performance, J Appl Phys, 120 (2016) 054501.
[53] D. Sacchetto, Q. Jeangros, G. Christmann, L. Barraud, A. Descoeudres, J. Geissbühler, M. Despeisse, A. Hessler-Wyser, S. Nicolay, C. Ballif, ITO/MoO_x/a-Si:H(i) hole-selective contacts for silicon heterojunction solar cells: Degradation mechanisms and cell integration, IEEE J Photovolt, 7 (2017) 1584-1590.
[54] M.A. Green, Solar cells: Operating principles, technology, and system applications, Prentice-Hall, Englewood Cliffs, NJ, USA, 1982.
[55] M.A. Green, Intrinsic concentration, effective densities of states, and effective mass in silicon, J Appl Phys, 67 (1990) 2944-2954.
[56] J. Zhao, A. Wang, S. Robinson, M. Green, Reduced temperature coefficients for recent high-performance silicon solar cells, Progress in Photovoltaics: Research and Applications, 2 (1994) 221-225.
[57] M.A. Green, Solar cell fill factors: General graph and empirical expressions, Solid State Electronics, 24 (1981) 788-789.
[58] C. Luderer, C. Messmer, M. Hermle, M. Bivour, Transport losses at the TCO/a-Si: H/c-Si heterojunction: Influence of different layers and annealing, IEEE J Photovolt, 10 (2020) 952-958.
[59] D. Kane, R. Swanson, Measurement of the emitter saturation current by a contactless photoconductivity decay method, 18th IEEE Photovoltaic Specialists Conference, (1985) 578–583.
[60] S.M.F. Zhang, J.P. Seif, T.G. Allen, R. Basnet, A.H.T. Le, I. Perez-Wurfl, Z. Hameiri1, Temperature- and illumination-dependent characterization of solar cells using Suns-V_{OC}(T) and I-V(T), 48th IEEE Photovoltaic Specialists Conference, (2021).
[61] R. Varache, C. Leendertz, M. Gueunier-Farret, J. Haschke, D. Muñoz, L. Korte, Investigation of selective junctions using a newly developed tunnel current model for solar cell applications, Sol Energ Mat Sol C, 141 (2015) 14-23.